International Journal of Engineering and Geosciences
https://dergipark.org.tr/en/pub/ijeg
e-ISSN 2548-0960

GIS-Based Analysis of Land Surface Characteristics and Urban Heat Islands in Metropolitan Cities of India

Dr. Rupesh Kumar Gupta[*1]

[1] *University of Delhi, Department of Continuing Education and Extension, India, Email: gisrs2004@gmail.com*

Cite this study: Gupta, R.K. (2025). GIS-Based Analysis of Land Surface Characteristics and Urban Heat Islands in Metropolitan Cities of India. International Journal of Engineering and Geosciences, 2025, 10(3), 440-455.

https://doi.org/10.26833/ijeg.1638818

Keywords
Urbanization
UHI
LST
Built-up Land
GIS

Research Article

Received:12.02.2025
1.Revised: 07.03.2025
2.Revised: 14.03.2025
Accepted:14.03.2025
Published:01.10.2025

Abstract

This study compares the Urban Heat Island (UHI) phenomenon in two Indian metropolitan cities: Lucknow and Delhi. This study helps to understand the comparative impact of urbanisation on the UHI effect in mid-sized and large urban cities using multi-temporal satellite data and index-based Analysis. MODIS satellite data were used to examine the UHI, while Landsat 8 data helped extract the land surface features of both cities. Various indices, such as NDVI, MBI, MNDWI, and NDBaI, were utilised to study the land surface characteristics of the study area using GIS-based tools and methods. The study findings indicate that about 18.15% of Lucknow is classified as a High Potential Urban Heat Island (UHI) Zone, compared to approximately 17.17% in Delhi. Land surface temperatures (LST) in Lucknow rose from 38.11°C and 30.41°C in 2000 to 46.17°C and 39.15°C in 2023. Similarly, in Delhi, LST values increased from 38.35°C and 24.49°C in 2000 to 47.27°C and 32.93°C in 2023. These zones are typically found in locations with high built-up land density and unplanned development activities. The study identifies a negative correlation between the UHI and the presence of green and blue spaces, which can help reduce the intensity of the UHI. The research emphasises the importance of understanding and managing the UHI effect in highly urbanised areas, as this knowledge will assist policymakers and stakeholders in enhancing livability and sustainability within cities.

1. Introduction

Urban areas are increasingly emerging as dynamic economic hubs and focal points for development, primarily driven by rapid urbanisation worldwide. As rural populations migrate toward cities for better employment opportunities, education, and healthcare, urban spaces transform into vibrant centres of innovation and activity. In 2018, the global urbanisation rate reached 55%, and it is projected that by 2050, 68% of the world's population will live in urban areas. This shift highlights the importance of well-planned infrastructure, sustainable development practices, and smart city solutions to accommodate swelling urban populations. Countries like India, China, and Nigeria are predicted to account for 35% of the increase in the global urban population between 2018 and 2050 [1]. According to the 2011 Indian census, India's urban population was 377 million, with an urbanisation rate of 31.1%. By 2050, this number is expected to rise by 416 million. However, the rapid expansion of cities also presents several challenges, including pollution, the formation of slums, and uncontrolled construction. These activities negatively impact the microclimate of urban areas, contributing to issues like urban heat islands and heat waves [2-8].

The urban microclimate refers to the environmental conditions in cities, shaped by various elements such as vegetation, land cover materials, urbanisation, and building design [9-10]. The complex interactions among surface materials, vegetation, and urban buildings influence the microclimate, affecting humidity, air temperature, and thermal comfort [11-12]. The microclimatic variations in urban areas also contribute to the UH) effect.

A UHI effect is a phenomenon where urban or metropolitan areas become noticeably warmer than nearby rural regions. [13]. This temperature difference is primarily caused by increased urbanisation and human activity within cities, resulting in distinct heat islands

with significant temperature variations between urban and rural environments [14-15].

Several factors contribute to the UHI effect, including replacing natural vegetation with heat-absorbing and heat-retaining surfaces such as concrete and asphalt. The heat generated by human activities—such as industrial operations, transportation, and energy consumption—exacerbates this effect [16-17]. Metropolitan regions often have insufficient greenery and vegetation, intensifying heat absorption and restricting the natural cooling effects of evapotranspiration[18-19]. The UHI effect is also affected by economic activities in these areas; increased temperatures in urban settings compared to their surroundings are primarily caused by heightened economic activity [20]. UHIs represent a significant environmental challenge associated with urbanisation and human activities. These phenomena affect the Environment, energy consumption, and public health. Heatwaves in urban areas can lead to a rise in heat-related health issues and fatalities, mainly affecting vulnerable groups like older adults and those living in low-income communities. [21].

Several studies have highlighted the role of land surface characteristics in land surface temperature. A survey of Bursa using Landsat images revealed a decrease in green vegetation alongside a significant increase in LST, with temperature differences of 5–6 °C between city centres and vegetated areas and up to 10 °C in densely urbanised regions[22]. Li et al. evaluated the Accuracy of Landsat 8-like land surface temperature generated using spatiotemporal fusion algorithms by combining Landsat 8 and MODIS data. Their findings demonstrated that the ESTARFM algorithm achieved the highest Accuracy (R^2 = 0.915, RMSE = 3.661 K), providing reliable high-resolution LST data for analysing UHI formation and LST variations[23]. A study in Saudi Arabia examined the impact of urbanisation on LST from 2002 to 2022, revealing a rise in LST from 25.08 °C to 54.42 °C in 2018 to 26.08 °C–56.31 °C in 2022, highlighting the land use changes as key contributors to UHI formation[24]. A UHI study in Raipur, India, showed a continuous increase in LST at a rate of less than 1% per annum, with UHI intensifying from a 2.6°C difference in 1995 to 3.63°C in 2016, particularly in industrial areas and regions with bare land [25]. An LST study in Punjab, India, using downscaled MODIS land surface temperature data, showed significantly higher temperatures in urban built-up cores (38.87 °C) compared to suburban (35.85 °C) and rural areas (32.41 °C) [26]. While these studies have mainly contributed to understanding UHI formation and its drivers, most have focused on single-city analyses or regional trends. This study compares UHI formation in two prominent Indian metropolitan cities, Lucknow and Delhi. By using MODIS satellite data to examine UHI intensities and Landsat 8 data to extract land surface features, this research aims to evaluate spatial and temporal variations of LST. The objectives of this research are as follows:

1. To evaluate the LST trends from 2000 to 2023.
2. To assess the UHI Effect on both the cities
3. Map and analyse the land surface characteristics of the study area.
4. To identify the relationship between UHI intensity and land surface characteristics.

Applying geospatial technologies has proven instrumental in analysing the LST and Land surface characteristics. These advanced methods facilitate comprehensive mapping, assessment, and interpretation of urban heat patterns and surface characteristics. [27-34].

2. Materials and Methods

2.1. Study Area

Delhi is a sprawling metropolis covering approximately 1,483 square kilometres in northern India as part of the National Capital Region (NCR). Its topography is marked by two distinct geographical features: the Delhi Ridge, an extension of the Aravalli Hills that acts as a natural shield against desertification, and the Yamuna floodplains, which provide fertile land but are susceptible to seasonal flooding. The city has undergone extensive urbanisation, with a landscape dominated by high-density residential and commercial areas, industrial zones, and green spaces like the Ridge Forest and Biodiversity Parks. This transformation has influenced local climatic conditions, contributing to the UHI effect.

Delhi experiences a humid subtropical climate (Koppen: Cwa) with extreme seasonal variations. According to the climate data provided by the Indian Meteorological Department, from April to June, Summers in Delhi are intensely hot, with temperatures frequently exceeding 45°C, further exacerbated by the dense built-up Environment. Winters, lasting from December to February, are cold and dry, with temperatures dropping to 2-4°C and frequent occurrences of thick fog. The monsoon season, spanning June to September, brings an average annual rainfall of 700-800 mm, often leading to waterlogging and urban flooding in low-lying areas.

Lucknow, the capital of Uttar Pradesh, spans approximately 631 square kilometres and lies within the fertile Gangetic Plain. Unlike Delhi, which has a mix of ridges and floodplains, Lucknow's topography is predominantly flat, making it well-suited for agricultural expansion and urban development. The Gomti River, which flows through the city centre, is crucial in shaping its Environment, affecting local weather patterns and groundwater availability. While the river supports the ecosystem of the cities, low-lying areas near it are prone to waterlogging during heavy monsoons.

The city experiences a humid subtropical climate (Koppen: Cwa), similar to Delhi but with relatively higher humidity and rainfall levels. As per the Indian Meteorological Department's data, from April to June, Summers see temperatures ranging between 40-45°C, though slightly lower than Delhi due to the moderating effect of moisture in the air. Winters are cold from December to February, with minimum temperatures dropping to 4-6°C, but they remain milder than in Delhi. From June to September, the monsoon season brings an annual rainfall of 900-1,000 mm, making Lucknow wetter than Delhi. The presence of the Gomti River and

associated wetlands contributes to localised cooling effects, creating distinct microclimates within the city. However, the higher humidity makes summers more uncomfortable, and seasonal flooding remains a concern in certain areas.

Delhi and Lucknow(Figure 1) were chosen for this study due to their shared humid subtropical climate, high population density, and rapid urbanisation, making them ideal for a comparative analysis of land surface changes. As capital cities—Delhi, India and Lucknow, Uttar Pradesh—both experience significant infrastructure expansion, environmental stress, and population pressure. With nearly 17 million residents, Delhi is a highly urbanised metropolis, while Lucknow, with a population of 4.6 million, is undergoing rapid growth while retaining peri-urban characteristics(Census of India, 2011). Their topography, built-up intensity, and green space distribution allow a detailed examination of the relationship between land use and LST within the same climatic zone. A comparative overview of the study areas is shown in Table 1.

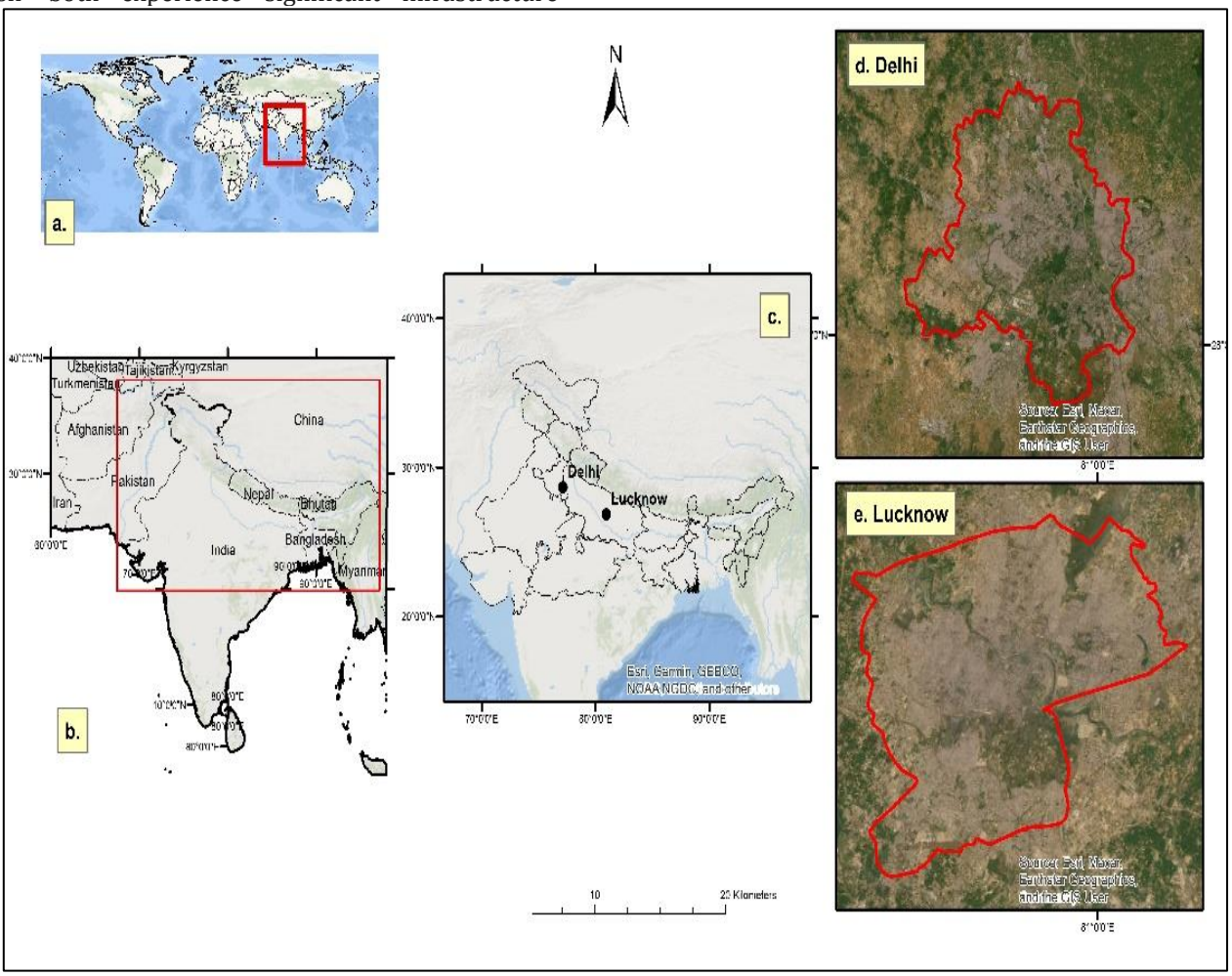

Figure 1. Study Area with (a) Location of Indian Subcontinent in the World; (b) Location of India in the Indian Subcontinent; (c) Location of Delhi and Lucknow in India; (d) Location Map of Delhi; (e) Location Map of Lucknow

Table 1. Comparative Overview of Study Areas

Parameter	Delhi	Lucknow	Source
Geographical Area	About 1,483 sq. km	About 631 sq. km	Survey of India
Topography	Ridge (Aravalli Hills) and Yamuna floodplains	Predominantly flat Gangetic plains with the Gomti River	Google Earth
Climate Type (Köppen)	Humid Subtropical (Cwa)	Humid Subtropical (Cwa)	Koppen
Mean Annual Temperature Extremes	Maximum: 20.1°C–39.9°C Minimum: 27.7°C - 7.5°C	Mean Maximum: 21.4°C - 39.9 °C Mean Minimum: 26.7°C - 7.8 °C	Indian Meteorological Department
Annual Rainfall	700–800 mm (Monsoon: June–September)	900–1,000 mm (Monsoon: June–September)	Indian Meteorological Department
Major Water Body	Yamuna River	Gomti River	Google Earth
Population (Census 2011)	~17 million	~4.6 million	Census of India

2.2. Data Sources

Satellite imagery obtained from NASA Earth Data and USGS Earth Explorer platforms was the primary data source for this study. The imagery was from Landsat 8 OLI, the Thermal Infrared Sensor (TIRS), and the MODIS Terra Sensor. Details of the data used are presented in Table 2.

Table 2. Geospatial Datasets used

Satellite	Spatial Reso.	Bands	Sensors	Cloud Cover	Time	Sources
Landsat 8	30 m	3, 4, 5, 6, and 10	OLI & TIRS	<30%	June 2023	USGS Earth Explorer
MODIS	1 km	31	Terra	<30%	June 2023 June 2010 June 2000	NASA Earth Data

2.3. Methods

Following data procurement, GIS-based techniques and processes were employed to examine and interpret the information. MODIS Terra data was utilised to determine the Land Surface Temperatures of the cities [35-37]. MODIS data was preferred for the LST study because MODIS offers frequent cloud-free observations, pre-processed LST products, and both daytime and nighttime thermal data, making it ideal for analysing diurnal and seasonal UHI variations [38-39]. While its spatial resolution is lower than Landsat, it has been widely used for the study of LST and UHI across the world [40-43]. For the land surface characteristics study, Landsat 8 Collection 2 Level-2 (L2) Surface Reflectance (SR) products were used[44– 45]. These L2 products are atmospherically corrected using advanced algorithms to remove the effects of atmospheric gases, aerosols, and water vapour. Necessary pre-processing steps, including cloud masking and extracting relevant spectral bands, were conducted before further Analysis. The ArcGIS 10.8 Software was used to analyse land surface temperatures and characteristics. Satellite sensors capture the brightness temperatures, which can be transformed into Land Surface Temperatures (LST) using the following formula for the MODIS Terra sensor in GIS. The conversion formula is(Equation 1)

$$LST(°C) = DN * 0.02 - 273.15 \quad (1)$$

DN = Digital Number derived from the MODIS *LST* data

An index-based methodology investigated cities' Urban Heat Island (UHI) phenomenon and land surface characteristics. These indices differentiate built-up areas, vegetation, water bodies, bare land, urban heat island effects, and their spatial distribution. The following indices were specifically applied: The Urban Thermal Field Variance Index (UTFVI) was calculated to evaluate UHIs[46-49]. This index is computed using the formula(Equation 2):

$$UTFVI = 1 - (LST_{Mean}/LST_{Pixel}) \quad (2)$$

LST_{Pixel} = Pixel values of LST of different locations

LST_{Mean} = Mean value of LST

The UHI intensity classification based on the UTFVI is as follows: areas with a UTFVI value of less than 0.005 are classified as Low UHI zones, those with values between 0.005 and 0.02 fall under Medium UHI zones, and areas with a UTFVI greater than 0.02 are categorised as High UHI zones.

To distinguish built-up areas from the surrounding vegetation, the Normalised Difference Built-Up Index (NDBI) was applied using Landsat 8 data [50]. The formula for NDBI is (Equation 3):

$$NDBI = \frac{\text{Short wave Infrared} - \text{Near InfraRed}}{\text{Short wave Infrared} + \text{Near InfraRed}} \quad (3)$$

An enhanced version of the NDBI, the Modified NDBI [51], was employed to refine the built-up area extraction by accounting for the presence of vegetation. It is calculated by subtracting the NDVI from the standard NDBI (see equation 4):

$$\text{Modified NDBI} = NDBI - NDVI \quad (4)$$

This modified index improves the Accuracy of built-up land detection by adjusting for vegetation density, allowing for a more precise mapping of urban areas [51].

The Normalised Difference Vegetation Index (NDVI) was used to study the vegetative cover across the study areas [52-57]. This index, derived from the near-infrared and red bands (Equation 5), provides valuable insight into vegetation's health and distribution in urban and rural settings.

$$NDVI = \frac{\text{Near Infrared} - \text{Red}}{\text{Near Infrared} + \text{Red}} \quad (5)$$

To identify water bodies and differentiate them from surrounding land features, the Modified Normalized Difference Water Index (MNDWI) was utilised [58]. This index helps isolate water bodies by using the green and short-wave infrared bands, which are particularly sensitive to water. The formula for MNDWI is(Equation 6):

$$MNDWI = \frac{\text{Green} - \text{Short wave Infrared}}{\text{Green} + \text{Short wave Infrared}} \quad (6)$$

The Normalised Difference Bareness Index (NDBaI) was used to extract bare land from surrounding land features [59]. This index utilises short-wave infrared and thermal bands to identify bare, undeveloped land within urban and peri-urban areas, which are essential for mapping areas with minimal vegetation or built infrastructure. The formula for NDBaI is(Equation 7):

$$NDBaI = \frac{\text{Short wave Infrared} - \text{Thermal}}{\text{Short wave Infrared} + \text{Thermal}} \quad (7)$$

The indices were calculated using GIS tools and statistical techniques, and the area was defined and extracted to analyse land surface characteristics and urban heat exposure. The threshold values of each index were determined using the Natural Jenks method and manual histogram analysis. The detailed flowchart of the methodology adopted is depicted in Figure 2.

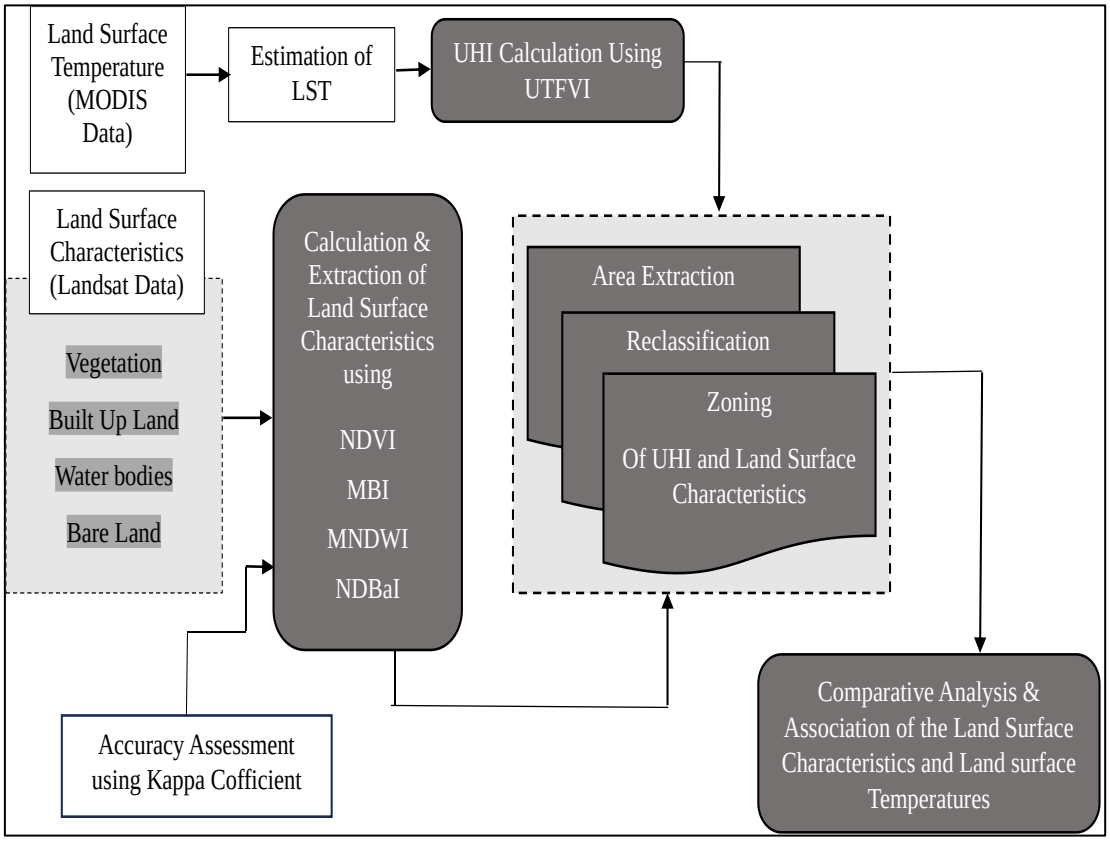

Figure 2. Methodology Flowchart

3. Results

Satellite datasets were utilised to analyse land surface characteristics through an index-based approach. The temporal variation of LST was examined using MODIS data. The results from both analyses provided a comparative assessment of these factors for Lucknow and Delhi.

3.1 Land Surface Characteristics

The land surface characteristics were studied using Landsat data, providing an overview of key features such as water bodies, vegetation, built-up land, and bare land. These features play a crucial role in influencing surface temperatures and the intensity of the UHI effect. Analysing these characteristics helps understand the spatial distribution of land cover types and their impacts.

3.1.1 Vegetation Cover

The Normalised Difference Vegetation Index (NDVI) uses infrared and red bands to distinguish vegetation from surrounding land cover. It serves as a tool for monitoring vegetation cover in any area. High NDVI values denote healthy vegetation, while low values are linked to other land cover types. Figure 7 illustrates the spatial distribution of dense and healthy vegetation cover in Delhi and Lucknow, as identified by NDVI mapping. The Histogram of the NDVI analysis (Figure 3) facilitated the evaluation of the threshold values for NDVI. Areas with values (Table 3) above 0.28849(for Delhi) and 0.2034(for Lucknow) were classified as regions of high vegetation.

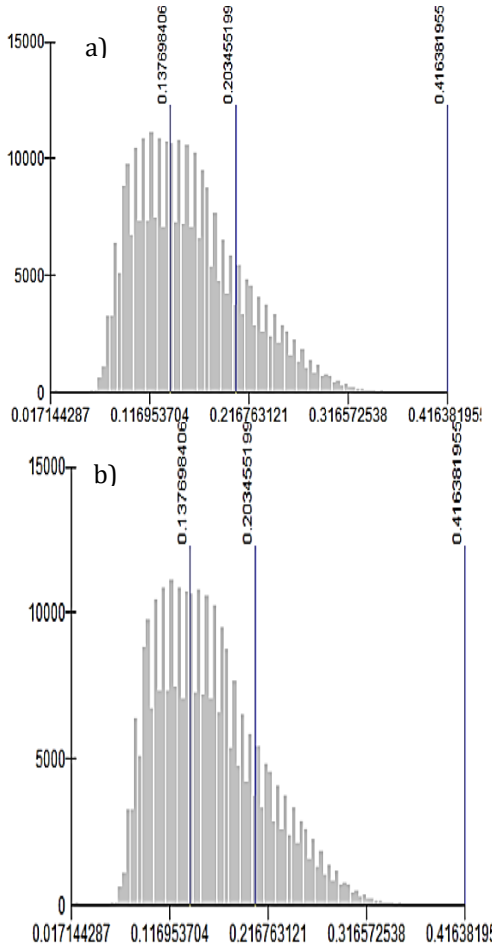

Figure 3: NDVI Histograms of (a). Delhi (b) Lucknow

Table 3: Threshold Values for Vegetation

City	Vegetation Threshold Value
Delhi	>0.2884
Lucknow	>0.2034

Areas such as forests and urban regions with significant vegetation, including cantonments and riverbanks, exhibit the highest NDVI values. In this comparison, Delhi has the highest NDVI score at 0.585, whereas Lucknow's NDVI is 0.416 (see Table 6). The NDVI analysis showed that 28.29% of Delhi exhibits high NDVI values. These zones are found mainly in the peri-urban parts of Northern and Southern Delhi, Delhi Cantonment, near the Yamuna River, and localised areas of Model Town, PUSA Hill Forest, Kamla Nehru Ridge, Yamuna Biodiversity Park, and Dhirpur Wetland. In comparison, approximately 21.16% of high vegetation density was identified in areas surrounding JNU and Lucknow, which includes locations such as Kukrail Forest, Cantonment, Research Designs and Standards Organization (RDSO), the outskirts along Hardoi Road, Janeshwar Park, and the Gomti River.

3.1.2 Built-Up Area

The Modified Built-Up Index (MBI) is an effective tool for identifying built-up areas, as it differentiates built-up regions from surrounding land cover types (Figure 7). After mapping the MBI values, a histogram analysis (Figure 4) was done to find the threshold values and identify the built-up areas. For Delhi, the values above -0.2361, whereas for Lucknow, those above -0.1876 were classified as the built-up areas (Table 4).

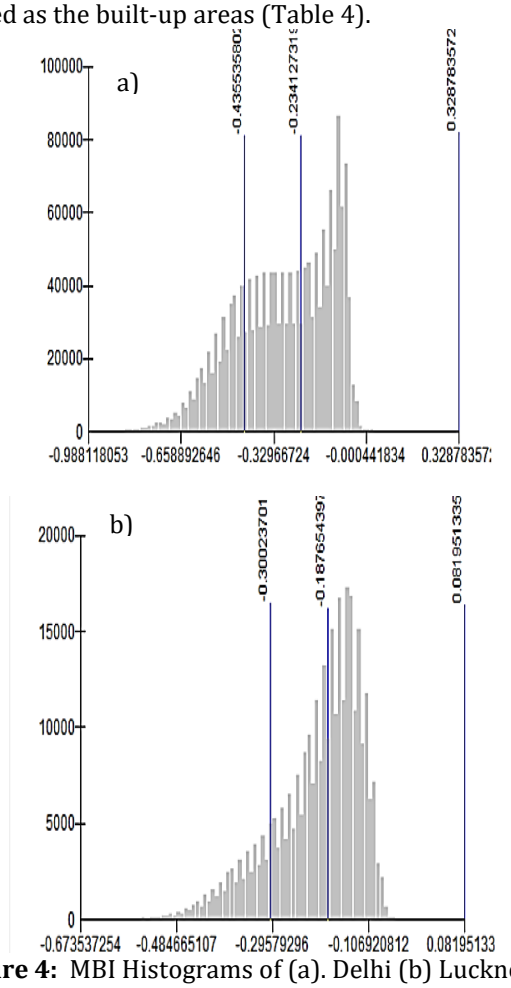

Figure 4: MBI Histograms of (a). Delhi (b) Lucknow

Table 4: Threshold Values for Builtup area

City	Built-up Area Threshold Value in MBI
Delhi	>-0.2361
Lucknow	>-0.1876

Lower MBI values indicate a variety of land uses, while higher values signify the presence of built-up areas. Major cities such as Delhi and Lucknow show high MBI scores of 0.328 and 0.081, respectively, suggesting high-density built-up regions (see Table 6).

In Lucknow, the areas with the highest MBI values include Chowk, Thakurganj, Balaganj, Aminabad, Rakabganj, Aishbagh, Saadatganj, Khadra, Daliganj, Alambagh, Krishnanagar, Aliganj, Indiranagar, and Kamta. In contrast, Delhi has comparatively higher MBI values in areas such as Shahdara, North East District, Sanjay Nagar, Uttam Enclave, Paharganj, Chandni Chowk, Karol Bagh, Patel Nagar, and Patparganj. Regarding the built-up portions of the cities, Lucknow has 54.84% of its total area with high MBI values, while Delhi has 51.13%.

3.1.3 Water Bodies

The presence of water bodies greatly influences the Surface Heat Islands in cities. The Modified Normalized Difference Water Index (MNDWI), which utilises the Green and Short-Wave Infrared Bands, effectively identifies water bodies. MNDWI values range from -1 to +1: negative values indicate other land use categories, while values approaching +1 signify the presence of a water body. Areas with MNDWI values (Table 5) above -0.0049(for Delhi) and -0.00520(for Lucknow) from the Histogram (Figure 5) were identified as the areas having waterbodies.

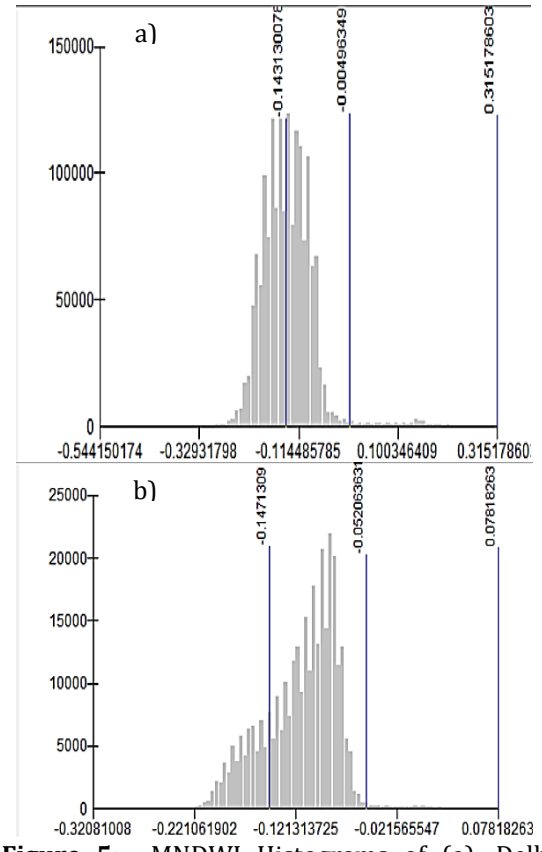

Figure 5: MNDWI Histograms of (a). Delhi (b) Lucknow

Table 5: Threshold Values for Waterbody

City	Water Body Threshold Value in MNDWI
Delhi	>-0.0049
Lucknow	>-0.0520

During the Analysis of MNDWI for Delhi and Lucknow, high values were observed in areas with substantial water bodies, such as lakes, rivers, or wetlands (Figure 7). The Gomati River, Kathauta Lake, Sahara Lake, Janeshwar Mishra Park Lake, and Indira Canal recorded the highest Mean Normalized Difference Water Index (MNDWI) values in Lucknow at 0.078. In comparison, the Yamuna River, Sahibi River, Bhalswa Lake, Yamuna Biodiversity Park Lake, Neeli Jheel, and other areas in Delhi had the highest MNDWI values at 0.315 (Table 6). Water bodies constituted 4.75% of the total area of Delhi, while Lucknow covered 6.08% of the total area.

3.1.4 Bare Land

The NDBaI is a tool used to identify the presence of bare land by analysing the short-wave infrared and thermal bands. Higher NDBaI values, typically around +1, indicate a more significant percentage of bare land, while other land use patterns correlate with values that deviate from +1. After the Histogram analysis(Figure 6), the values above -0.1809 for Delhi and above -0.2557 for Lucknow were identified as the Bare Land(Table 6).

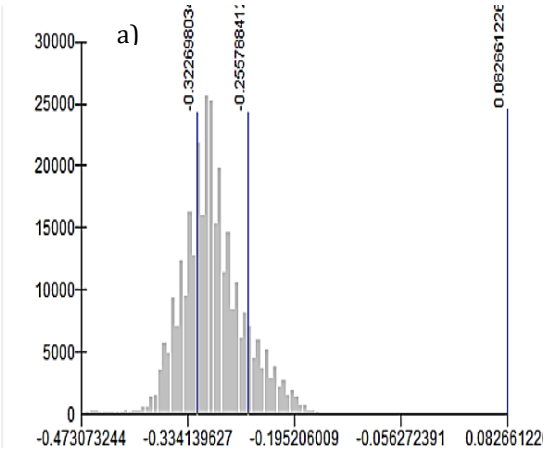

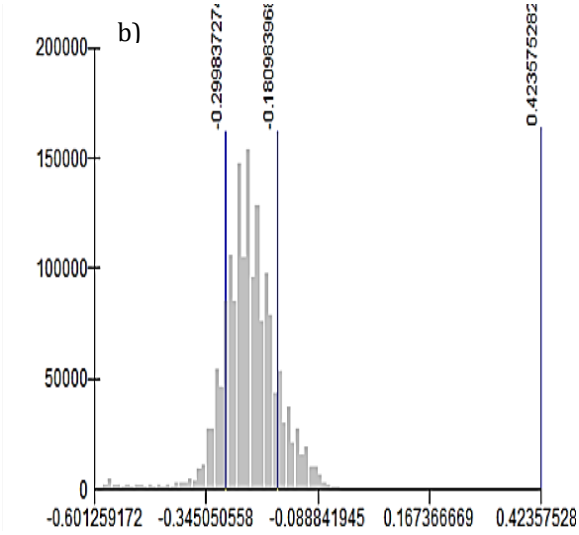

Figure 6: NDBaI Histograms of (a). Delhi (b) Lucknow

Table 6: Threshold Values for Bare Land

City	Bare Land Threshold Value in NDBaI
Delhi	>-0.1809
Lucknow	>-0.2557

In Lucknow, the NDBaI value was recorded at 0.082, indicating the presence of bare land across several regions, including Ghaila, Dubagga, and Amausi and other peri-urban zones such as IIM Road, Gudamba, Kursi Road, and Sarojini Nagar (Figure 7). On the other hand, Delhi demonstrated a higher NDBaI value of 0.423, particularly across its northern, northwestern, and western peri-urban districts. Areas such as Bankoli, Bawana, and Ladpur showed prominent readings, likely reflecting urban sprawl and the conversion of green spaces into developed land (Table 7). Bare land accounts for 16.72% of the total area of Lucknow, while in Delhi, it constitutes 12.14%.

Table 7. Values of indices

Index	Lucknow		Delhi	
	Maximum	Minimum	Maximum	Minimum
NDVI	0.416	0.0171	0.585	-0.136
MBI	0.081	-0.673	0.328	-0.988
NDBaI	0.082	-0.473	0.423	-0.601
MNDWI	0.078	-0.320	0.315	-0.544

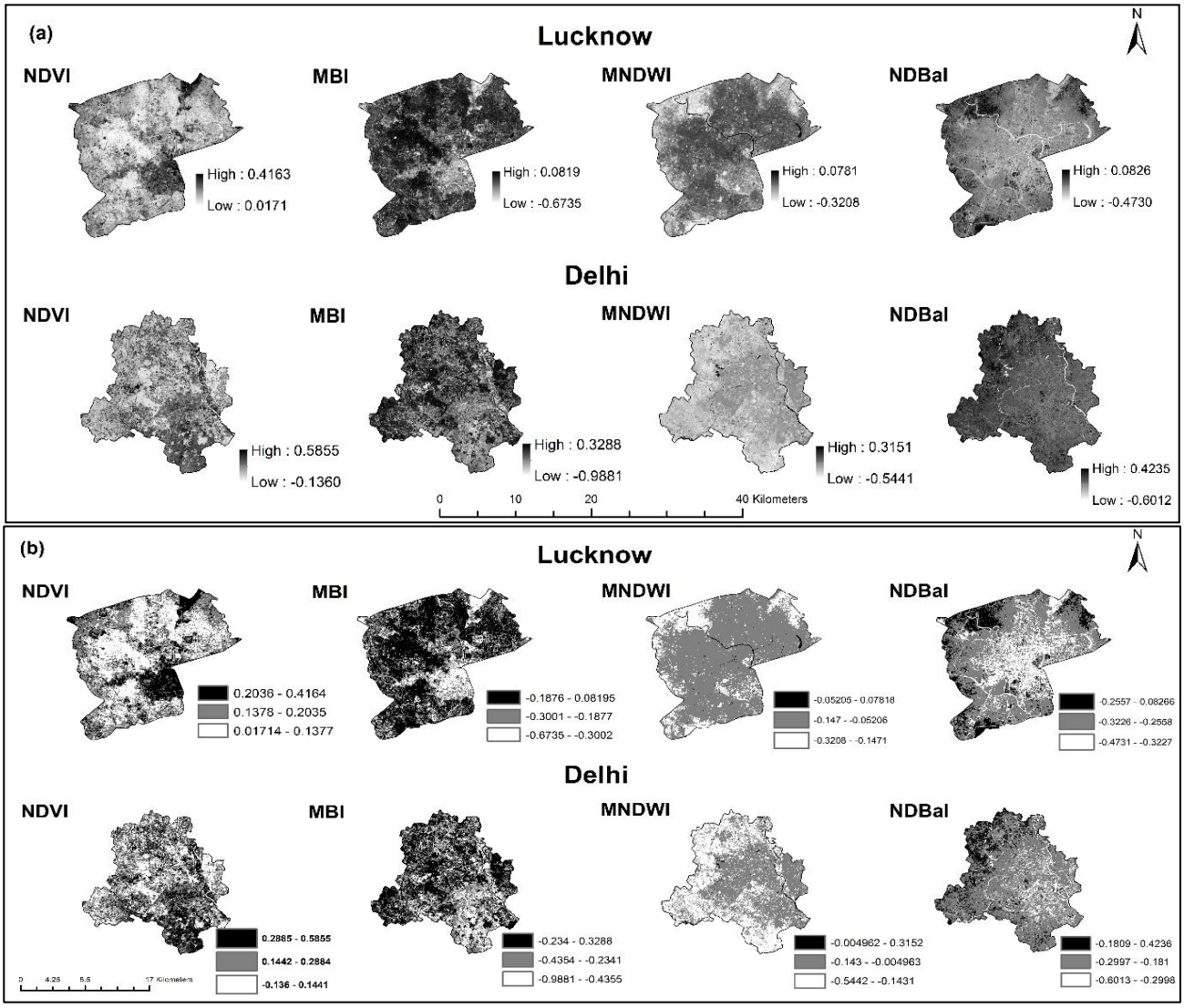

Figure 7. Indices mapping (a) Index Maps without reclassification (b) Index Maps showing threshold Values

3.2 Accuracy Assessment of Index-Based Classification

The accuracy assessment of the index-based classification was conducted using ArcGIS 10.8 with the "Create Accuracy Assessment Points" tool, ensuring a systematic and unbiased evaluation of the results. Fifty sample points for each index were generated using a stratified random sampling approach, ensuring even distribution across different land cover types within the study areas. This method reliably represented various land surface features, reducing potential bias during validation. The classification of NDVI, MBI, MNDWI, and NDBaI was manually verified against high-resolution satellite imagery available in Google Earth Pro. The NDVI classification effectively captured vegetated areas, confirming the presence of high-density vegetation in the identified zones, yielding an overall accuracy of 87.6% and a kappa coefficient of 0.85. The MBI assessment accurately distinguished built-up regions, with minimal misclassification observed in mixed-use areas, resulting in an accuracy of 85.2% and a kappa coefficient of 0.82. Similarly, the MNDWI results correctly mapped water bodies, with a strong correlation between classified water zones and actual water features in both cities, achieving an accuracy of 88.4% and a kappa coefficient of 0.86. The NDBaI classification demonstrated high reliability in detecting bare land, with peri-urban expansion areas aligning well with the classified bare land zones, recording an accuracy of 86.9% and a kappa coefficient of 0.84. The classification results were highly accurate, with substantial agreement observed based on kappa statistics(Table 8).

Table 8. Accuracy Assessment

Index	Overall Accuracy (%)	Kappa Coefficient	Correctly Classified (Out of 50 Samples)	Misclassified
NDVI	87.60%	0.85	44	6
MBI	85.20%	0.82	42	8
MNDWI	88.40%	0.86	47	3
NDBaI	86.90%	0.84	45	5

3.3 Land Surface Temperatures

Figure 8 illustrates the thermal properties of the land in both cities based on LST calculations. In Lucknow, the LST has increased over time, with maximum temperatures rising from 38.11°C in 2000 to 46.17°C in 2023 and minimum temperatures from 30.41°C to 39.15°C. This indicates a significant warming trend, suggesting intensified UHI effects and changes in surface characteristics. In contrast, Delhi has also experienced a considerable increase in LST, with maximum temperatures rising from 38.35°C in 2000 to 47.27°C in 2023, and minimum temperatures from 24.49°C to 32.93°C. The overall temperature variation in Delhi remains broader than in Lucknow, with a temperature span of 14.34°C in 2023 compared to 7.02°C in Lucknow. This wider variation in Delhi suggests more significant spatial differences in land cover, urban density, and surface materials, contributing to localised heating effects and differential thermal responses across the city (Table 9).

Table 9. Land Surface Temperatures (in °C)

City	2000		2010		2023	
	Maximum	Minimum	Maximum	Minimum	Maximum	Minimum
Lucknow	38.11	30.41	37.39	32.67	46.17	39.15
Delhi	38.35	24.49	41.99	31.61	47.27	32.93

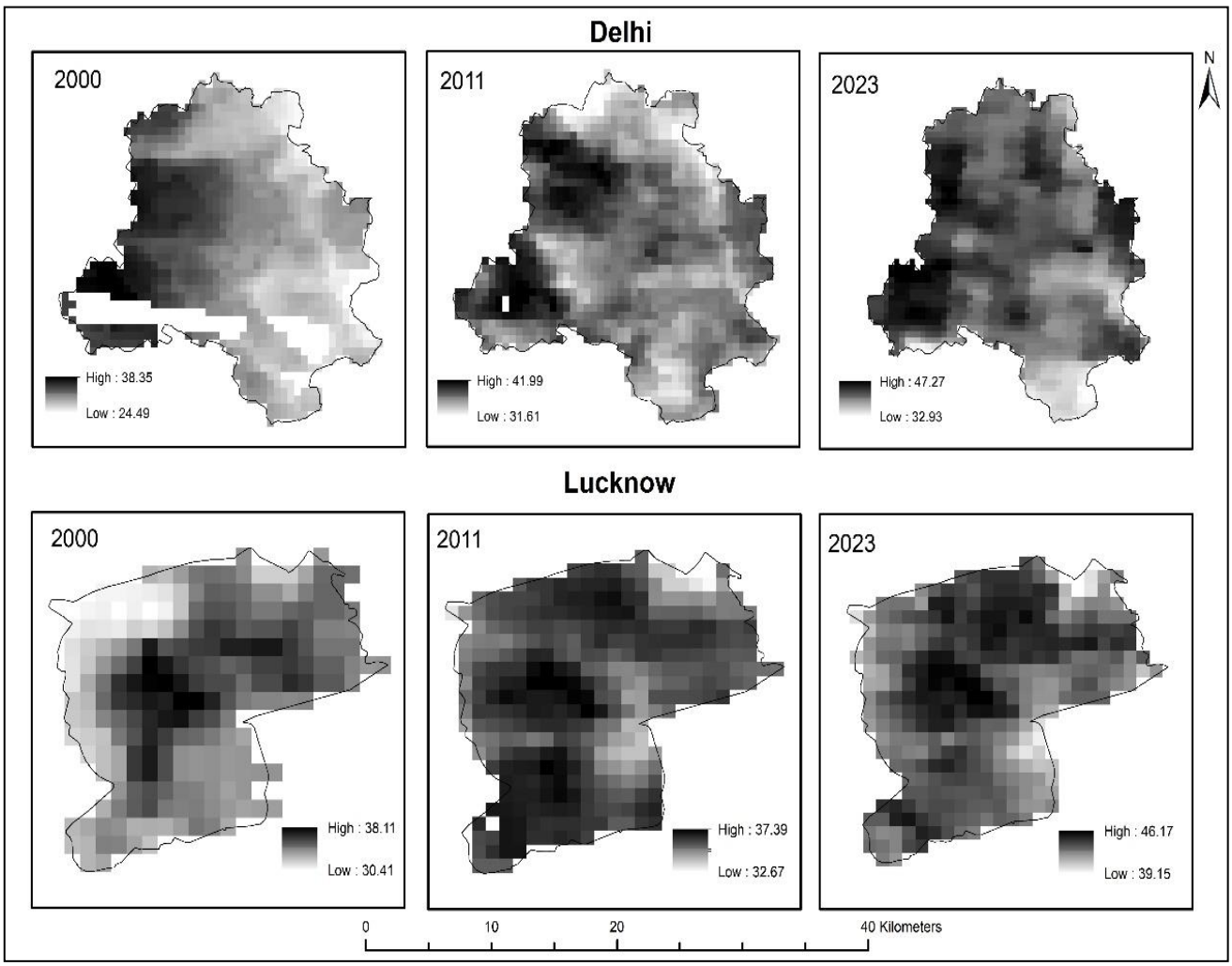

Figure 8. LST Map of Delhi and Lucknow

3.4 Urban Heat Island

The UTFVI (Urban Thermal Field Variability Index) for Delhi and Lucknow was calculated for the year 2023, including the Land Surface Temperature (LST) values and the mean LST values derived from satellite imagery, to map the current UHIs for both cities (Figure 9). The computed UTFVI was categorised into UHI Zones as High, Medium, and Low potential zones. The results indicate that both cities experience a significant UHI effect. As shown in Table 5, Lucknow has approximately 18.15% of its total land area classified as High Potential, while Delhi has about 17.17% of its location in the same category (Table 10).

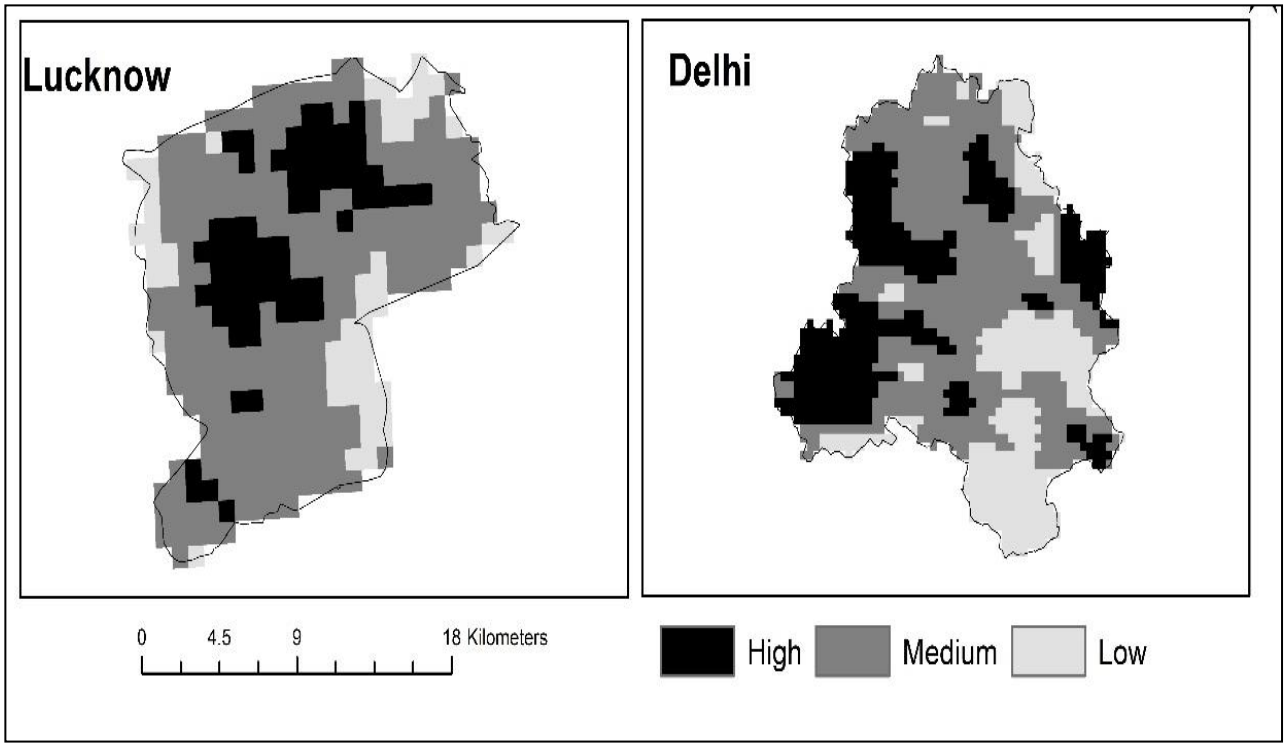

Figure 9. UHI Potential Zones of Lucknow and Delhi for 2023

Table 10. Area Statistics of UHI Potential Zones

City	Low Potential UHI Zone (% of total area)	Moderate Potential UHI Zone (% of total area)	High Potential UHI Zone (% of total area)
Lucknow	30.11	51.74	18.15
Delhi	40.20	42.63	17.17

The urban heat potential has excellent variability across the city of Lucknow. The UHI effect is less pronounced in areas with a large concentration of green spaces, such as Kukrail Forest, the Cantonment Area, and RDSO, as well as near water bodies like Kathauta Lake and Sahara Lake. In contrast, older parts of the city, including Chowk, Khadra, Thakurganj, and Aliganj in both the cis and trans-Gomati regions, experience intensified urban heat, primarily due to their limited vegetation. These areas also exhibit higher land surface temperatures. The extent of arid land surrounding the city has helped to moderate thermal comfort levels.

The UHI patterns of Delhi vary between older, densely constructed areas and those with substantial greenery and water bodies. Due to inadequate planning, older neighbourhoods such as Karol Bagh, Paharganj, and Chandni Chowk are particularly susceptible to the UHI effect. In contrast, areas with water bodies, like the Yamuna River, and dense vegetation, such as Kamla Nehru Ridge and PUSA Hill Forest, serve as heat sinks, helping to moderate temperatures. The peri-urban areas around Delhi, particularly in the western region, experience higher land surface temperatures. This is mainly due to the open nature of the area, which is sparse in vegetation.

4. Discussion

The relationship between land surface characteristics and LST has been analysed for both cities, revealing a significant association between land cover types and temperature variations. The index-based classification of land cover types has helped us understand how vegetation, built-up areas, barren lands, and water bodies influence surface temperatures.

In Lucknow (Figure 10), areas with dense vegetation, such as the Kukrail Forests and Cantonment zones, exhibited relatively lower temperatures, ranging between 39-40°C. This temperature moderation can be attributed to extensive tree cover and green spaces, which help in evapotranspiration and reduce surface heat absorption. In contrast, densely built-up areas, including commercial and residential clusters, recorded much higher LST values, reaching up to 46°C. The higher temperature in these areas is due to the UHI effect, where concrete structures, asphalt roads, and reduced vegetation contribute to heat retention. The barren lands in the city's western parts, including peri-urban zones with ongoing construction and sparse vegetation, exhibited moderate LST values, ranging around 43°C.

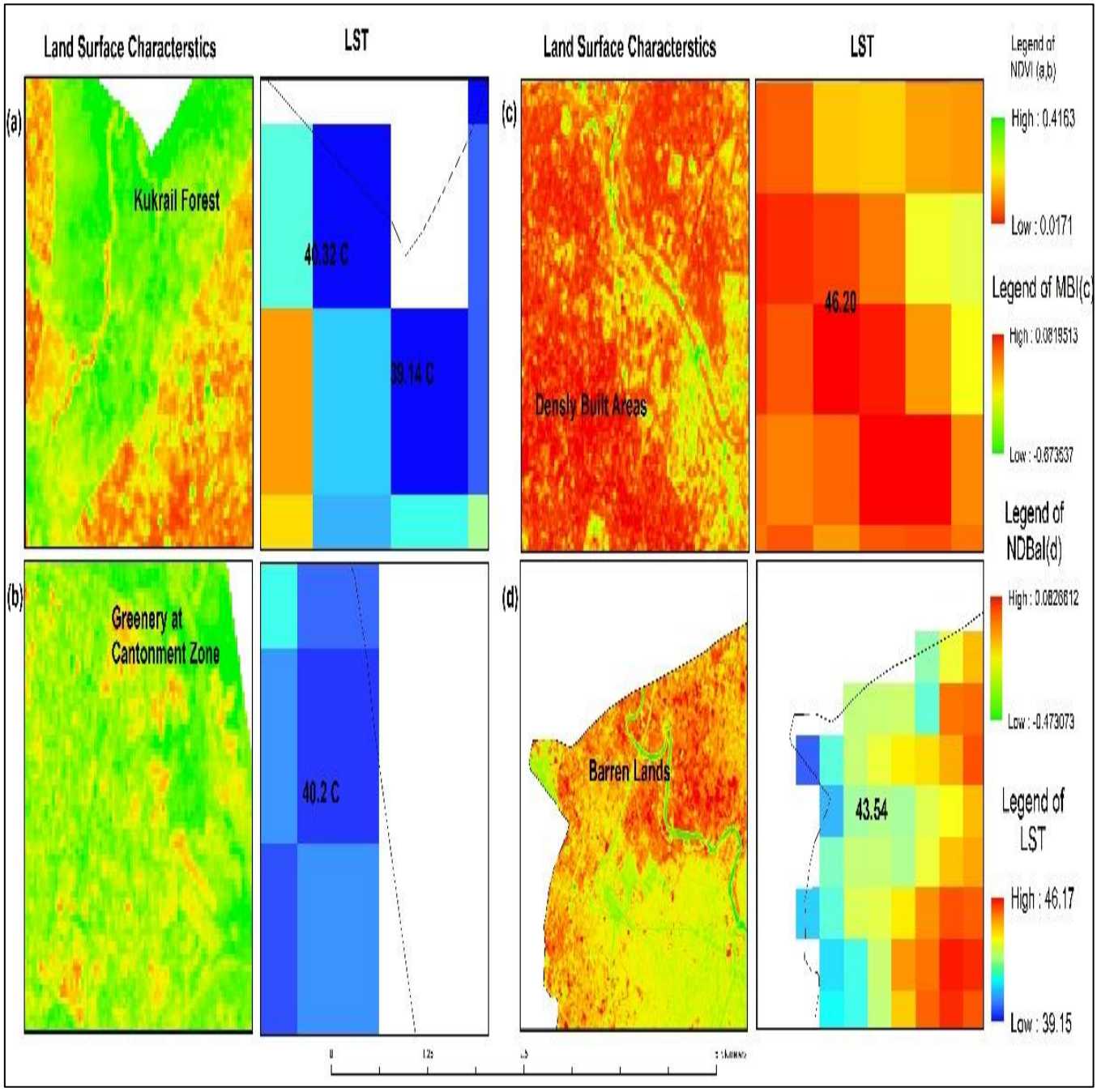

Figure 10. LST and Land Surface Characteristics Association of Lucknow

A similar trend was observed in Delhi (Figure 11), with variation in LST values, likely due to the city's diverse land cover types and complex urban morphology. This variation may be attributed to a mix of dense built-up areas, green spaces, and water bodies, contributing to localised differences in temperature. A similar trend was observed in Delhi (Figure 6) but with more significant variation due to the complex urban morphology and diverse land cover types. The densely built-up areas of East Delhi, which include commercial hubs, industrial zones, and high-density residential clusters, recorded the highest LST values, reaching 46.17°C. These regions experience intense urban heat island effects due to high impervious surface cover, limited green spaces, and high anthropogenic activities. Areas with significant vegetation cover, such as Pusa, JNU, and the Ridge Forests, experienced much lower temperatures, ranging between 34-36°C. These green zones mitigate urban heat by providing shade and facilitating evaporative cooling. Similarly, the Yamuna River and its surrounding floodplains exhibited relatively lower temperatures, approximately 33°C, highlighting the cooling influence of water bodies. The presence of moisture in these areas helps moderate temperatures and counteract heat accumulation in surrounding urban spaces. However, the western parts of Delhi, particularly in peri-urban areas with extensive barren lands, recorded higher temperatures of 43-44°C. These areas, characterised by sparse vegetation and dry soil conditions, absorb and retain heat, leading to increased surface temperatures.

Overall, the study demonstrates a strong correlation between LST and land surface characteristics, emphasising the role of vegetation, water bodies, and urbanisation patterns in shaping local temperature variation.

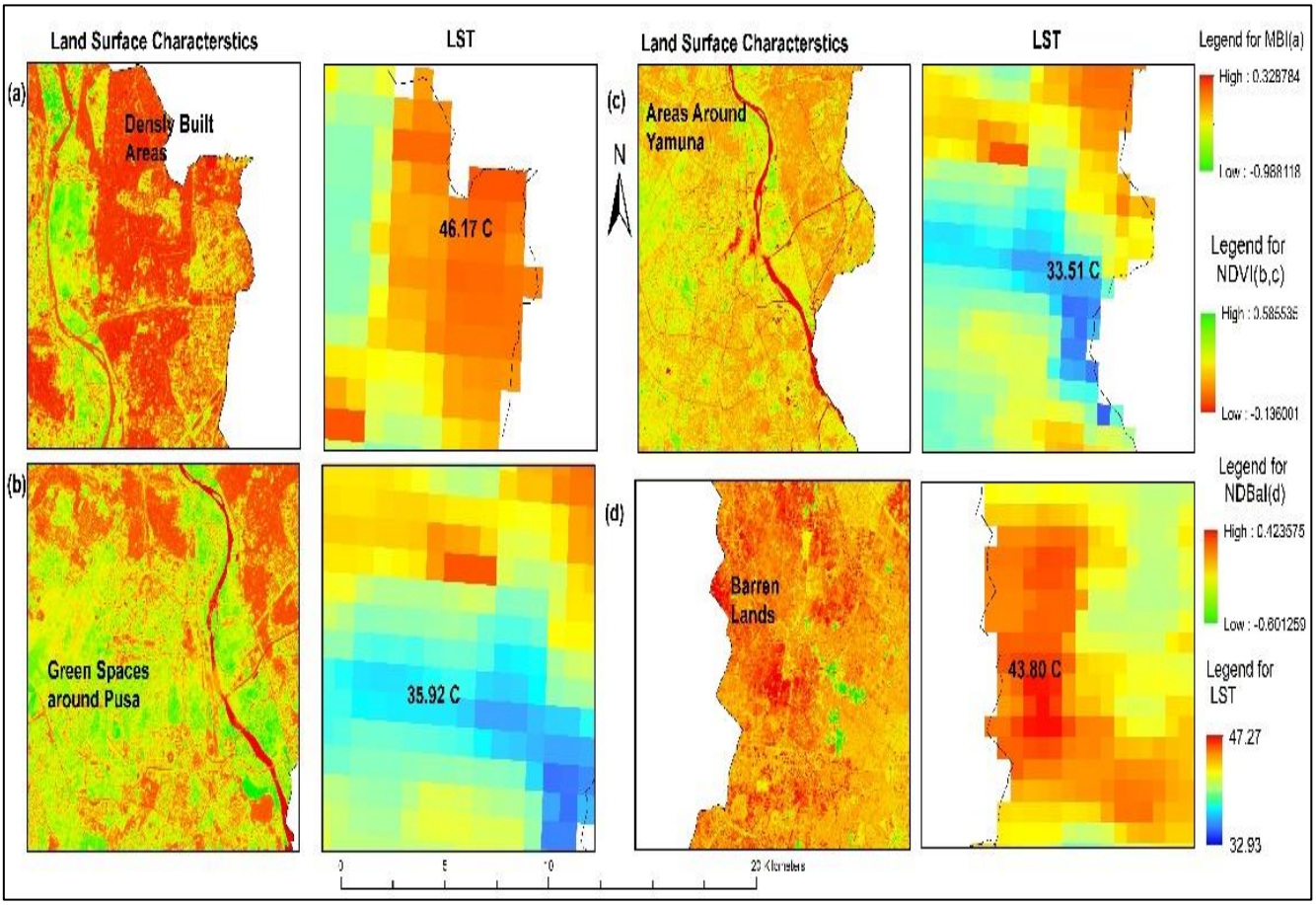

Figure 11. LST and Land Surface Characteristics Association of Delhi

5. Conclusion

This study provides valuable insights into the dynamics of urban microclimates and the impact of land surface characteristics on temperature changes in Lucknow and Delhi. The land surface temperature trends over the years (Table 4) further emphasise these findings. In Lucknow, LST values have increased from 38.11°C and 30.41°C in 2000 to 46.17°C and 39.15°C in 2023, indicating a substantial temperature rise. Similarly, Delhi has experienced a temperature escalation, with LST increasing from 38.35°C and 24.49°C in 2000 to 47.27°C and 32.93°C in 2023. Areas in these cities characterised by uncontrolled concrete growth exhibit higher land surface temperatures, which contribute to the formation of urban heat islands.

In contrast, the presence of vegetation and water bodies helps to absorb heat in metropolitan areas. A comparative analysis indicates the formation of UHI in dense urban areas of Lucknow and Delhi, where limited vegetation cover is a contributing factor. The mapping and Analysis of land surface characteristics further support these findings by identifying the spatial distribution of built-up land, vegetation, water bodies, and barren land. High-density urban regions such as Aminabad, Aliganj, and Charbagh in Lucknow and central Delhi exhibit the highest LST values, while areas with significant vegetation cover, including Pusa Hill Forest, Kamla Nehru Ridge, and Kukrail Forest, experience lower temperatures due to evapotranspiration and shading effects. This study establishes a relationship between UHI intensity and land surface characteristics, demonstrating that built-up expansion and decreasing vegetation correlate with higher LST values.

The findings of this study align with previous research on UHIs and LST variations in rapidly urbanising cities. Several studies have established that urbanisation, built-up expansion, and declining vegetation cover are the primary drivers of rising LST and the intensification of UHIs. Nayak et al. [60] analysed UHI effects in various cities and found that dense built-up areas experience temperature increases of 2–10°C compared to surrounding vegetated regions. This aligns with our results, where densely developed sections of Lucknow and Delhi show higher LST values, reaching 46–47°C, while vegetated regions remain cooler (33–36°C). Similarly, Grover & Singh. [61] examined UHI trends in Delhi and found that vegetation and water bodies help mitigate high temperatures, supporting our observation that areas such as Kamla Nehru Ridge and the Yamuna floodplains exhibit lower temperatures. Singh et al. [62] used remote sensing techniques to assess UHI patterns in Lucknow. They found that high-density built-up regions such as Aminabad, Aliganj, and Charbagh exhibited the highest LST values, ranging from 33–42°C, a trend reflected in our findings. Several researches conducted [63-64] on Beijing's urban heat island effect demonstrated that UHI intensity correlates strongly with increased built-up areas and bare land, similar to our results showing that barren lands in western Delhi and Lucknow contribute to higher LST values. Gupta [65]

found that water bodies, such as the Yamuna River, act as thermal regulators, a pattern evident in our study where water bodies in both cities recorded lower LST values. While studying the LST of Raipur City, Guha et.al.. and others [66 -67] found a stronger positive correlation between LST and Bare Land (0.64), indicating that bare surfaces contribute significantly to temperature rise. Ghanbari et al. & others [68-70] found a strong relationship between LST and spectral indices, with built-up and barren areas showing the highest correlation with surface temperature. Pandey et.al.. [71] found a negative relationship between LST and vegetation indices in both summer and winter, indicating cooler temperatures in vegetated areas. In contrast, NDBI showed a strong positive correlation with LST, highlighting the impact of built-up and bare surfaces on increasing temperatures. Similar trends were also found in the case of Delhi and Lucknow in this study, where the higher temperatures were mainly found in areas with a high density of built-up land and bare land, while lower temperatures were centred around the waterbodies and vegetation cover.

This study highlights the crucial need to comprehend urban microclimates to mitigate the effects of urban heat islands. Understanding these localised temperature variations can help implement effective strategies to cool urban spaces, such as increasing green cover and enhancing sustainable urban planning. Reducing the intensity of UHIs improves the quality of life and contributes to energy conservation and public health[72-73]. However, the study is limited by the availability and resolution of satellite data, which may not adequately capture fine-scale spatial variations. Incorporating higher-resolution imagery, along with validation using in-situ meteorological observations, could enhance the understanding of urban heat dynamics and support more targeted interventions. Moreover, official meteorological datasets from the India Meteorological Department (IMD) are not available through open-access platforms, and limited funding restricts the procurement of such datasets or the collection of primary meteorological data. Future research should focus on integrating high-resolution remote sensing with localized ground observations to improve accuracy and support data-driven urban climate resilience planning.

Acknowledgement

The authors sincerely thank the Survey of India, NASA, USGS, ISRO, and Google Earth for helping in this research work through the open source data supply.

Author contributions

Rupesh Kumar Gupta: Conceptualisation, Methodology, Data curation, Software, Validation, Original draft preparation, Writing, Reviewing, and Editing.

Conflicts of interest

The authors declare no conflicts of interest.

References

1. United Nations, Department of Economic and Social Affairs, Population Division (2018). World urbanization prospects: The 2018 revision, online edition.
2. Gupta, R. K. (2024). Geospatial and statistical analysis of land surface temperature and land surface characteristics of Jaipur and Ahmedabad cities of India. Journal of Geoscience and Environment Protection, 12(8), 1–19.
3. Handayani, W., & Rudiarto, I. (2014). Dynamics of urban growth in Semarang metropolitan – Central Java: An examination based on built-up area and population change. Journal of Geography and Geology, 6(4).
4. Patil, R., & Datta, M. (2022). Spatio-temporal analysis of climate change in India: A theoretical perspective. Advanced Geomatics, 2(1), 7–13.
5. Li, X., Mitra, C., Dong, L., & Yang, Q. (2018). Understanding land use change impacts on microclimate using the Weather Research and Forecasting (WRF) model. Physics and Chemistry of the Earth, Parts A/B/C, 103, 115–126.
6. Patra, S., Sahoo, S., Mishra, P., & Mahapatra, S. K. (2018). Impacts of urbanisation on land use/cover changes and its probable implications on local climate and groundwater level. Journal of Urban Management, 7(2), 70–84.
7. Prayudha, W., Pradnyapasa, D., & Nurhasana, R. (2022). Urban configuration of Thamrin City buildings in Jakarta. IOP Conference Series: Earth and Environmental Science, 1108(1), 012062.
8. Murenzi Gilbert, K., & Shi, Y. (2024). Using GlobeLand30 data and cellular automata modelling to predict urban expansion and sprawl in Kigali City. Advanced Remote Sensing, 4(1), 46–57.
9. Funsho, S., Busayo, D., & Kehinde, O. (2018). The effects of urbanisation on the micro-climate of Minna urban area. Journal of Geography, Environment and Earth Science International, 15(1), 1–13.
10. Kurniati, R., Kurniawati, W., Dewi, D., & Astuti, M. (2021). Measurement of thermal comfort in urban public spaces, Semarang, Indonesia. Pertanika Journal of Science and Technology, 29(3).
11. Meshram, Y., Deshpande, S., & Valsson, S. (2022). Study on the appropriate ground cover configuration of open spaces to mitigate urban heat island effect.
12. Prayoga, S., & Kusumawanto, A. (2019). Thermal comfort simulation on Cik Ditiro corridor. Dimensi (Journal of Architecture and Built Environment), 46(1), 67–78.
13. Liu, L., & Zhang, Y. (2011). Urban heat island analysis using the Landsat TM data and ASTER data: A case study in Hong Kong. Remote Sensing, 3(7), 1535–1552.
14. He, Q., & Reith, A. (2023). A study on the impact of green infrastructure on microclimate and thermal comfort. Pollack Periodica, 18(1), 42–48.
15. Lee, S., Moon, H., Choi, Y., & Yoon, D. (2018). Analysing thermal characteristics of urban streets using a thermal imaging camera: A case study on

commercial streets in Seoul, Korea. Sustainability, 10(3), 519.
16. Montaseri, M., Masoodian, S., & Guo, X. (2022). Evaluation of surface urban heat island intensity in arid environments (case study: Isfahan metropolitan area).
17. Akbari, H., Pomerantz, M., & Taha, H. (2001). Cool surfaces and shade trees to reduce energy use and improve air quality in urban areas. Solar Energy, 70(3), 295–310.
18. Sailor, D., & Lu, L. (2004). A top-down methodology for developing diurnal and seasonal anthropogenic heating profiles for urban areas. Atmospheric Environment, 38(16), 2737–2748.
19. Arnfield, A. J. (2003). Two decades of urban climate research: A review of turbulence, exchanges of energy and water, and the urban heat island. International Journal of Climatology, 23(1), 1–26.
20. Tang, C. (2022). A study of the urban heat island effect in Guangzhou. IOP Conference Series: Earth and Environmental Science, 1087(1), 012015.
21. Reid, C. E., O'Neill, M. S., Gronlund, C. J., Brines, S. J., Brown, D. G., Diez-Roux, A. V., ... & Schwartz, J. (2009). Mapping community determinants of heat vulnerability. Environmental Health Perspectives, 117(11), 1730–1736.
22. Yamak, B., Yağcı, Z., Bilgilioğlu, B. B., & Çömert, R. (2020). An investigation of the effect of urbanisation on land surface temperature in Bursa. International Journal of Engineering and Geosciences, 6(1), 1–8.
23. Li, S., Wang, J., Li, D., Ran, Z., & Yang, B. (2021). Evaluate Landsat 8-like land surface temperature by fusing Landsat 8 and MODIS land surface temperature product. Processes, 9(12), 2262.
24. Mallick, J., & Alqadhi, S. (2024). Explainable artificial intelligence models for proposing mitigation strategies to combat urbanisation impact on land surface temperature dynamics in Saudi Arabia. Urban Climate, 59, 102259.
25. Guha, S. (2017). Dynamic analysis and ecological evaluation of urban heat islands in Raipur city, India. Journal of Applied Remote Sensing, 11(3), 1.
26. Mukherjee, S., Joshi, P. K., & Garg, R. D. (2016). Analysis of urban built-up areas and surface urban heat islands using downscaled MODIS-derived land surface temperature data. Geocarto International, 32(8), 900–918.
27. Başara, A. C., Tabar, M. E., Gülsün, S., & Şişman, Y. (2BC). Monitoring urban sprawl in Atakum District using CORINE data. Advanced Geomatics, 2(2), 49–56.
28. Arif, N. (2023). Thermal comfort analysis in urban areas using remote sensing and geographic information system. IOP Conference Series: Earth and Environmental Science, 1190(1), 012013.
29. Gupta, R., & Parashar, D. (2020). Estimation of land surface temperature in the urbanised environment using multi-resolution satellite. Uttar Pradesh Geographical Journal, 25, 15–28.
30. Unel, F. B., Kusak, L., & Yakar, M. (2023). GeoValueIndex map of public property assets generating via Analytic Hierarchy Process and Geographic Information System for Mass Appraisal: GeoValueIndex. Aestimum, 82, 51-69..
31. Polat, Z. A., Kırtıloğlu, O. S., & Kayalık, M. (2023). Evolution and future trends in global research on geographic information system (GIS): A bibliometric analysis. Advanced GIS, 3(1), 22–30.
32. Tezel, D., Aydemir, T., Taşkın, C., & Gündoğan, Ü. (2024). 3D modeling and land management in protected areas: Fethiye-Göcek SEPA. Advanced Geomatics, 2(2), 37–48.
33. Yalçın, C., Öztürk, S., & Kumral, M. (2022). Heat maps of U-TH enrichments in open source coded geographical information systems (GIS); Arıklı (Çanakkale, Turkey) District. Advanced GIS, 2(1), 46–51.
34. Prasad, P., & Satyanarayana, A. (2022). Assessment of outdoor thermal comfort using Landsat 8 imageries with machine learning tools over a metropolitan city of India. [Journal Name Missing].
35. Phan, T., Kappas, M., & Degener, J. (2016). Estimating daily maximum and minimum land air surface temperature using MODIS land surface temperature and ground truth data in Northern Vietnam. Remote Sensing, 8(12), 1002.
36. Orhan, O., & Yakar, M. (2016). Investigating land surface temperature changes using Landsat data in Konya, Turkey. The International Archives of the Photogrammetry, Remote Sensing and Spatial Information Sciences, 41, 285-289.
37. Zhang, H., Zhai, F., Zhang, G., Ma, Y., Yang, K., & Ye, M. (2018). Daily air temperature estimation on glacier surfaces in the Tibetan Plateau using MODIS LST data. Journal of Glaciology, 64(243), 132–147.
38. Hassan, S., Edicha, J., & Kabiru, U. (2016). Analysis of the pattern of land degradation in Okaba, Kogi State, Nigeria. Annals of the Social Science Academy of Nigeria, 20(1).
39. Huang, C., Kim, S., Song, K., Townshend, J., Davis, P., Altstatt, A., … & Musinsky, J. (2009). Assessment of Paraguay's forest cover change using Landsat observations. Global and Planetary Change, 67(1–2), 1–12.
40. Orhan, O., & Yakar, M. (2016). Investigating land surface temperature changes using Landsat data in Konya, Turkey. The International Archives of the Photogrammetry, Remote Sensing and Spatial Information Sciences, 41, 285-289.
41. Spruce, J., Smoot, J., Ellis, J., Hilbert, K., & Swann, R. (2013). Geospatial method for computing supplemental multi-decadal US coastal land use and land cover classification products, using Landsat data and C-CAP products. Geocarto International, 29(5), 470–485.
42. Dapke, P. (2024). A comparative analysis of machine learning techniques for LULC classification using Landsat-8 satellite imagery. International Journal of Engineering and Geosciences.
43. Tao, Y., Lan, G., She, L., Pang, L., & Kong, F. (2018). Dynamic monitoring of land cover in the Dongting Lake area between 1995–2015 with Landsat imagery. The International Archives of the

Photogrammetry, Remote Sensing and Spatial Information Sciences, XLII-3, 1651–1656.
44. Zhu, Z., & Woodcock, C. (2014). Continuous change detection and classification of land cover using all available Landsat data. Remote Sensing of Environment, 144, 152–171.
45. Gull, A., & Mahmood, S. (2022). Spatiotemporal analysis and trend prediction of land cover changes using the Markov Chain model in Islamabad, Pakistan. Advanced GIS, 2(2), 52–61.
46. Mogaraju, J. K. (2024). Machine learning assisted in the land surface temperature (LST) prediction based on major air pollutants over the Annamayya District of India. International Journal of Engineering and Geosciences, 9(2), 233–246.
47. Sobrino, J. A., & Irakulis, I. (2020). A Methodology for Comparing the Surface Urban Heat Island in Selected Urban Agglomerations Around the World from Sentinel-3 SLSTR Data. Remote Sensing, 12(12), 2052.
48. Toy, S., Yılmaz, S., & Yılmaz, H. (2007). Determination of bioclimatic comfort in three different land uses in Erzurum, Turkey. Building and Environment, 42(3), 1315–1318.
49. Morsy, S., & Hadi, M. (2022). Impact of land use/land cover on land surface temperature and its relationship with spectral indices in Dakahlia Governorate, Egypt. International Journal of Engineering and Geosciences, 7(3), 272–282.
50. Zha, Y., Gao, J., & Song, N. (2003). Use normalised difference built-up index to map urban areas from TM imagery automatically. International Journal of Remote Sensing, 24(3), 583–594.
51. He, C., Shi, P., Xie, D., & Zhao, Y. (2010). Improving the normalised difference built-up index to map urban built-up areas using a semiautomatic segmentation approach. Remote Sensing Letters, 1(4), 213–221.
52. Huang, X., Zhang, T., Yi, G., He, D., Zhou, X., Li, J., … & Miao, J. (2019). Dynamic changes of NDVI in the growing season of the Tibetan plateau during the past 17 years and its response to climate change. International Journal of Environmental Research and Public Health, 16(18), 3452.
53. Mao, D., Wang, Z., Liu, L., & Ren, C. (2012). Integrating AVHRR and MODIS data to monitor NDVI changes and their relationships with climatic parameters in northeast China. International Journal of Applied Earth Observation and Geoinformation, 18, 528–536.
54. Piao, S., Wang, X., Ciais, P., Zhu, B., Wang, T., & Liu, J. (2011). Changes in satellite-derived vegetation growth trend in temperate and boreal Eurasia from 1982 to 2006. Global Change Biology, 17(10), 3228–3239.
55. Reed, B., Brown, J., VanderZee, D., Loveland, T., Merchant, J., & Ohlen, D. (1994). Measuring phenological variability from satellite imagery. Journal of Vegetation Science, 5(5), 703–714.
56. Guliyev, İ., & Hüseynov, R. (2024). Comparative character and monitoring of some soil and vegetation parameters by remote sensing in the zone of Zangilan. Advanced Remote Sensing, 4(1), 28–35.
57. Erdoğan, A., Görken, M., Kabadayı, A., & Temizel, S. (2022). Evaluation of green areas with remote sensing and GIS: A Yozgat city centre case study. Advanced Remote Sensing, 2(2), 58–65.
58. Xu, H. (2006). Modification of normalised difference water index (NDWI) to enhance open water features in remotely sensed imagery. International Journal of Remote Sensing, 27(14), 3025–3033.
59. Zhou, Y., Yang, G., Wang, S., Wang, L., Wang, F., & Liu, X. (2014). A new index for mapping built-up and bare land areas from Landsat-8 OLI data. Remote Sensing Letters, 5(10), 862–871.
60. Nayak, S., Vinod, A., & Prasad, A. K. (2023). Spatial Characteristics and Temporal Trend of Urban Heat Island Effect over Major Cities in India Using Long-Term Space-Based MODIS Land Surface Temperature Observations (2000–2023). Applied Sciences, 13(24), 13323.
61. Grover, A., & Singh, R. (2015). Analysis of Urban Heat Island (UHI) about Normalised Difference Vegetation Index (NDVI): A comparative study of Delhi and Mumbai. Environments, 2(2), 125–138.
62. Singh, P., Kikon, N., & Verma, P. (2017). Impact of land use change and urbanisation on urban heat island in Lucknow city, Central India. A remote sensing-based estimate. Sustainable Cities and Society, 32, 100–114.
63. Zhou, D., Zhao, S., Liu, S., Zhang, L., & Zhu, C. (2014). Surface urban heat island in China's 32 major cities: Spatial patterns and drivers. Remote Sensing of Environment, 152, 51–61.
64. Yilmaz, H. M., Yakar, M., Mutluoglu, O., Kavurmaci, M. M., & Yurt, K. (2012). Monitoring of soil erosion in Cappadocia region (Selime-Aksaray-Turkey). Environmental Earth Sciences, 66, 75-81.
65. Gupta, R. K. (2024). Identifying urban hotspots and cold spots in Delhi using the Biophysical Landscape framework. Ecology Economy and Society–the INSEE Journal, 7(1), 137–155.
66. Guha, S., Govil, H., & Mukherjee, S. (2023). Long-Term Evaluation of Land Surface Temperature with Bare Surface Index and Surface Vegetation Index: A Case Study of a Central Indian City. Papers in Applied Geography, 9(4), 425–441.
67. Şenol, H. İ., Kaya, Y., Yiğit, A. Y., & Yakar, M. (2024). Extraction and geospatial analysis of the Hersek Lagoon shoreline with Sentinel-2 satellite data. Survey Review, 56(397), 367-382.
68. Ünel, F. B., Kuşak, L., Yakar, M., & Doğan, H. (2023). Coğrafi bilgi sistemleri ve analitik hiyerarşi prosesi kullanarak Mersin ilinde otomatik meteoroloji gözlem istasyonu yer seçimi. Geomatik, 8(2), 107-123.
69. Çelik, M. Ö., Kuşak, L., & Yakar, M. (2024). Assessment of groundwater potential zones utilizing geographic information system-based analytical hierarchy process, Vlse Kriterijumska Optimizacija Kompromisno Resenje, and technique for order preference by similarity to ideal solution methods: a case study in Mersin, Türkiye. Sustainability, 16(5), 2202.

70. Ayalke, Z., & Şişman, A. (2024). Machine learning based improved land cover classification using Google Earth Engine: Atakum, Samsun example. Geomatik, 9(3), 375-390.
71. Pandey, A., Mondal, A., & Guha, S. (2024). Assess the relationship of land surface temperature with nine land surface indices in a northeast Indian city using summer and winter Landsat 8 data. Cogent Engineering, 11(1).
72. Yakar, M., & Dogan, Y. (2019). 3D Reconstruction of residential areas with SfM photogrammetry. In Advances in Remote Sensing and Geo Informatics Applications: Proceedings of the 1st Springer Conference of the Arabian Journal of Geosciences (CAJG-1), Tunisia 2018 (pp. 73-75). Springer International Publishing.
73. Kaynarca, M. (2023). Extraction of building areas with the use of unmanned aerial vehicles, calculation of building roof slopes. Advanced UAV, 3(2), 136–141.